

# Classification of Large-Scale Environments that drive the formation of Mesoscale Convective Systems over Southern West Africa

Francis Nkrumah<sup>1,2</sup>, Cornelia Klein<sup>3,5</sup>, Kwesi Akumenyi Quagraine<sup>1,4</sup>, Rebecca Berkoh Oforiwaa<sup>2,6</sup>, Nana Ama Browne Klutse<sup>2,6</sup>, Patrick Essien<sup>1,2</sup>, Gandomè Mayeul Leger Davy Quenum<sup>2,7</sup> and Hubert Azoda Koffi<sup>6</sup>

<sup>1</sup>Department of Physics, University of Cape Coast, Private Mail Bag, Cape Coast, Ghana;

<sup>2</sup>African Institute of Mathematical Sciences (AIMS), Sector Remera, Kigali 20093, Rwanda;

<sup>3</sup>U.K. Centre for Ecology and Hydrology, Wallingford, United Kingdom

<sup>4</sup>Climate System Analysis Group (CSAG), ENGEU, University of Cape Town, Private Bag X3, Rondebosch, Cape Town 7701, South Africa

<sup>5</sup>Department of Atmospheric and Cryospheric Sciences, University of Innsbruck, Innsbruck, Austria

<sup>6</sup>Department of Physics, University of Ghana, Legon P.O. Box LG 63, Ghana

<sup>7</sup>National Institute of Water (NIW), University of Abomey-Calavi, Godomey, Cotonou 01 PB: 4521, Benin

*Correspondence to:* Francis Nkrumah ([francis.nkrumah@ucc.edu.gh](mailto:francis.nkrumah@ucc.edu.gh)) and Nana Ama Browne Klutse ([nklutse@ug.edu.gh](mailto:nklutse@ug.edu.gh))

**Abstract.** Mesoscale convective systems (MCSs) are frequently observed over southern West Africa (SWA) throughout most of the year. However, it has not yet been identified what variations in typical large-scale environments of the West African monsoon seasonal cycle may favour MCS occurrence in this region. Here, six distinct synoptic states are identified and are further associated with being either a dry season, pre-, post-, or peak-monsoon synoptic circulation type using self organizing maps (SOMs) with inputs from reanalysis data. We identified a pronounced annual cycle of MCS numbers with frequency peaks in June and September that can be associated with peak rainfall during the major and minor rainy seasons respectively across SWA. Comparing daily MCS frequencies, MCSs are most likely to develop during post-monsoon conditions featuring a northward-displaced moisture anomaly (0.42 MCSs per day), which can be linked to strengthened low-level westerlies. Considering that these post-monsoon conditions occur predominantly from September and into November, these patterns may in some cases be representative of a delayed monsoon retreat. On the other hand, under peak monsoon conditions, we observe easterly wind anomalies during MCS days, which reduce moisture content over the Sahel but introduce more moisture over the coast. Finally, we find all MCS-day synoptic states to exhibit positive zonal wind shear anomalies. Seasons with the strongest zonal wind shear anomalies are associated with the strongest low-level temperature anomalies to the north of SWA, highlighting that a warmer Sahel can promote MCS-favourable conditions in SWA. These significant positive zonal wind shear anomalies for MCS days illustrate the importance of zonal wind shear for MCS development in SWA throughout the year.

## 1 Introduction

The region of West Africa is subject to variability in rainfall on both spatial and temporal scales. Fundamentally, the rainfall pattern in West Africa is modulated by the annual change in the position of the

40 Intertropical Convergence Zone (ITCZ) and the West African Monsoon (WAM). Due to endemic poverty, lack of  
41 infrastructure and technology, rapid population increase, and significant fluctuation of the WAM, West Africa has  
42 been deemed one of the world's most susceptible regions to climate change (IPCC, 2014). The climate of southern  
43 West Africa (SWA) can be categorized into four seasonal stages: a dry season from December to February, two wet  
44 seasons lasting from April to June, and September to November, and the so-called little dry season in August (e.g.  
45 Thorncroft et al. 2011). Between March and June, when low-level winds are more westerly and the intertropical  
46 convergence zone (ITCZ) starts to move northward, the precipitable water peaks over SWA (Klein et al. 2021). The  
47 ITCZ retreats southward in September, creating the second rainy season, followed by a dry season from November  
48 to January.

49 One major atmospheric disturbance that contributes to the WAM is the presence of Mesoscale Convective  
50 Systems (MCSs) which supplies around 30-80 % of the total rainfall during the WAM (Klein et al. 2018). MCSs are  
51 organized thunderstorm clusters, often defined to have a minimum horizontal extent of the precipitating area of 100  
52 kilometres in at least one direction (Guo et al. (2022); Chen et al. (2022); Houze (2004)). Maranan et al. (2018) note  
53 that diverse MCS sub-groups such as squall- or disturbance lines, structured convective systems, and mesoscale  
54 convective complexes impact the hydro-climate of West Africa. In both the tropics and midlatitudes, MCS also  
55 contributes significantly to rainfall extremes, rendering them a substantial contributor to the hydrologic cycle (Feng  
56 et al. (2021); Li et al. (2020)). More studies have been motivated in recent decades by evaluating drivers that affect  
57 rainfall variability and intensity associated with MCSs (Baidu et al. (2022); Augustin et al. (2022)). MCSs, for  
58 instance, supply essential precipitation and, as a result, supply water to agriculturally productive regions in the  
59 tropics, particularly in semi-arid regions such as the Sahel (Nesbitt et al. (2006)).

60 However, relative to our understanding of MCS drivers in the Sahel, SWA has received less attention. The  
61 connections of MCSs to larger-scale atmospheric motion and states are both important and not fully understood for  
62 the southern region, hence, a better understanding of large-scale MCS drivers is important for improving  
63 precipitation prediction over SWA. Earlier research has suggested an increasing role of other types of less-organized  
64 rainfall in place of MCSs over the Guinea Coast (e.g. (Acheampong, 1982; Fink et al., 2006; Kamara, 1986;  
65 Omotosho, 1985), with MCS contribution to annual rainfall decreasing from 71% in the Soudanian to 56% in the  
66 coastal zone (Maranan et al 2018), emphasizing MCS importance across the SWA region. Maranan et al., 2018 also  
67 concluded that precipitable water and Convective Available Potential Energy (CAPE) determine where MCSs may  
68 occur in SWA, while zonal wind shear is a stronger predictor for distinguishing between small scattered convection  
69 and MCS-type development. Indeed, zonal wind shear intensification was found to be a major driver of increasing  
70 frequencies of the most intense Sahelian MCSs over the last three decades (Taylor et al., 2017), a mechanism that  
71 was similarly found to play a role for early-season MCS intensification in SWA (Klein et al 2021). Zonal wind  
72 shear, which is thought to modulate the storm-available supply of moist buoyant air, is also seen to be very critical  
73 to the organization of convective systems (e.g., Alfaro, 2017; Mohr & Thorncroft, 2006). Accordingly, propagating  
74 storms with longer-lasting organized precipitation systems were consistently found to be associated with strong  
75 vertical wind shear and higher values of CAPE in the Sahel (Hodges & Thorncroft, 1997; Laing et al., 2008; Mohr  
76 & Thorncroft, 2006).

77 Previous studies address the large-scale settings for WAM-related rainfall throughout the seasons (Sultan  
78 and Janicot, 2003) with less attention given to the importance of large-scale WAM modes and their effect on  
79 regional MCS frequencies in SWA. The role of regional MCS-centred environments in the initiation and  
80 development of MCSs in West Africa has been well studied (e.g., Klein et al. 2021; Vizy and Cook 2018; Schrage et  
81 al. 2006; Maranan et al. 2018). Vizy and Cook (2018) observed that the extension of vertical mixing to the level of  
82 free convection, as a result of surface heating, tends to initiate MCSs in an environment where the mid-tropospheric  
83 African easterly wave disturbance is located in the east. The vertical wind shear is enhanced as a result of the  
84 synoptic disturbance. Klein et al. (2021) suggested that heavy rainfall, due to cold MCSs during both dry and rainy  
85 seasons, occurs in an environment with stronger vertical wind shear, increased low-level humidity, and drier mid-  
86 levels. Unlike vertical wind shear, Maranan et al., (2018) suggested that thermodynamic conditions such as CAPE  
87 and Convective Inhibition (CIN) are of lesser importance for the horizontal growth of convective systems, although  
88 they indicate the potential of the initial vertical development of convective systems. Janiga and Thorncroft (2016)  
89 also suggested that CAPE, vertical wind shear and column relative humidity are the decisive large-scale  
90 environmental parameters that control the characteristics of convective systems. Based on radar and sounding  
91 observations aligned around 15°N, Guy et al. (2011) analyzed MCSs and their respective environmental conditions  
92 over three different regimes of West Africa (maritime, coastal, and continental). They concluded that MCSs tend to  
93 occur ahead of the African easterly wave (AEW) trough during the maritime and the continental regime, while they  
94 are mostly found behind the trough in the coastal regime.

95 It is not clear to what extent different large-scale patterns such as temperature, wind, humidity, and CAPE  
96 at different stages of the WAM drive the formation of MCSs over SWA. Hence, this study systematically classifies  
97 the different large-scale patterns across the WAM region and how they are associated with MCSs over SWA. For  
98 this purpose, a classification using a self organizing map (SOM; Kohonen 2001) analysis was carried out to  
99 characterize large-scale WAM patterns during the 1981-2020 period, which we subsequently grouped into days with  
100 MCS occurrence over SWA. The SOM is a clustering technique that is topologically sensitive and uses an  
101 unsupervised training method to cluster the training data (Lennard and Hegerl, 2014; Quagraine et al. 2019). This  
102 methodology thus allows us to identify favourable types of large-scale environments driving the formation of MCSs  
103 within different WAM stages.

104 The paper is organized as follows: Section 2 details the study area and data sources and how they were  
105 processed. In section 3, the SOM methodology and other needed statistics used to investigate the relationship  
106 between large-scale environment patterns and particular MCSs are presented. Section 4 discusses the main results,  
107 which include the common features and different types of large-scale patterns associated with MCSs. Section 5  
108 provides the summarized conclusions of the study.

## 109 **2 Data Sources and Processes**

### 110 **2.1 ERA5 Reanalysis Data and MCS Data**

111 The ECMWF fifth-generation atmospheric reanalysis (Hersbach et al., 2020), ERA5, was used as the main  
112 data source in this work. The dataset is generated using 41r2 of the Integrated Forecast System (IFS) model, based

113 on a four-dimensional variational data assimilation scheme, and takes advantage of 137 vertical model levels and a  
114 horizontal resolution of  $0.28125^\circ$  (31 km). The data provides hourly estimates of model integration. In this study,  
115 hourly zonal and meridional winds (650 and 925 hPa), specific humidity (925 hPa), temperature (925 hPa), and  
116 convective available potential energy (CAPE) in ERA5 during 1981–2020 were used to explore suitable large-scale  
117 environments for the development of MCSs in SWA ( $5\text{--}9^\circ\text{N}$ ,  $10^\circ\text{W}\text{--}10^\circ\text{E}$ ). The zonal and meridional wind, as well as  
118 specific humidity at 925 hPa, are used to understand the penetration of monsoon flow inland. The zonal wind  
119 difference between 925 hPa and 650 hPa is used as a zonal wind shear change indicator while the temperature at 925  
120 hPa is used to visualize Saharan heat low (SHL) differences.

121 The Meteosat Second Generation (MSG) cloud-top temperature data, which are available every 15 minutes  
122 from the Eumetsat archives online (<https://navigator.eumetsat.int/product/EO:EUM:DAT:MSG:HRSEVIRI>) was  
123 used in this study. Fifteen years of MCS snapshots (2004–18) detected from Meteosat Second Generation  $10.8\ \mu\text{m}$ -  
124 band brightness temperatures (Schmetz et al. 2002, EUMETSAT 2021) are used to define MCS days in this study.  
125 Following Klein et al. (2021), an MCS is defined here as a  $-50^\circ\text{C}$  contiguous cloud area larger than  $5000\ \text{km}^2$ . An  
126 "MCS day" is then defined as a day with at least 5 MCSs between 16 and 1900 UTC per day that is raining  $>5\text{mm}$   
127 within the SWA domain. This can include the same MCS at several timesteps in a day. Corresponding rainfall  
128 snapshots were sampled from the "high-quality precipitation" (HQ) field within the Integrated Multi-satellite  
129 Retrievals for Global Precipitation Measurement (IMERG; Huffman et al. 2019) dataset. Here, only land-based  
130 MCSs because MCSs over land are fundamentally more intense and deep than its counterpart over the ocean (Mohr  
131 and Zipser 1996).

132

### 133 **3 Methodology**

#### 134 **3.1 Self-organising Maps (SOMs) analysis**

135 The study uses the self organizing map (SOM; Kohonen 1982, 2001) from SOM-PAK-3.1 software. The  
136 technique is used to identify archetype synoptic circulation patterns over the southern West Africa region by training  
137 a 9-node SOM with ERA5 daily mean 925 hPa geopotential height fields to produce 9 characteristic circulation  
138 patterns for the period 1981 to 2020. The geopotential height circulation pattern is used here mainly based on its  
139 physically realistic output spanning a range of circulation features found in the atmosphere (Hewitson and Crane,  
140 2002) and its ability to detect the West African Heat Low (WAHL) which is a key element of the West African  
141 monsoon system (Lavaysse et al. 2009; Biasutti et al. 2009). The SOM is mostly the preferred choice over other  
142 clustering methods such as the principal component analysis (PCA) or K-means because the data is not discretized  
143 and orthogonality is not forced or does not require subjective rotations to produce interpretable patterns. The main  
144 advantage of the SOM technique is its ability to deal with non-linear data (such as the continuum of atmospheric  
145 conditions) and can easily be visualized and interpreted (Reusch et al. 2005; Lennard and Hegerl, 2014). The steps  
146 within the technique can be broadly grouped into two stages, namely the training stage and the mapping stage.  
147 Earlier studies (e.g. Hewitson and Crane 2002; Kim and Seo 2016; Lee 2017; Rousi et al. 2015; Sheridan and Lee  
148 2012) have successfully used this technique in synoptic climatology to effectively preserve relationships between  
149 weather states while giving outputs that are readily understood and can be easily visualized as an array of classified

150 patterns. These classified patterns help in interpreting relationships between large-scale regional circulation patterns  
151 and local weather expressions and rainfall extremes (Hewitson and Crane 1996; Cassano et al. 2015; Wolski et al.  
152 2018). In this study, the SOM is randomly initialized allowing for hidden patterns and structure in the geopotential  
153 height at 925 hPa to be discovered while the algorithm iteratively updates the weights of the nodes to better  
154 represent the data. The strength of initializing the SOM this way lies also on its robustness to noise and outliers as a  
155 result of the algorithm applying a competitive learning structure to the data which then allows for the formation of  
156 distinct clusters. The SOM\_PAK algorithm allows the SOM process to minimize quantization and topological errors  
157 at the mapping stage when choosing the best SOM as outlined in Lennard and Hegerl (2014). However, there is a  
158 trade-off when choosing the size of the SOM, as this is dependent on the need to generalize circulation states for  
159 analyses or the need to capture predominant spatial characteristics that affect the local climate. Thus, in this study,  
160 we have tested several sizes of the SOM and have arrived at using a 9-node SOM. As depicted in Fig. S1 for a 9-  
161 node SOM, it is evident that some nodes are still redundant, and this is a compromise on states not being overly  
162 generalized while capturing the dominant spatial characteristics over the region. Here, we agree on six nodes, which  
163 allow distinct synoptic states to be reproduced while grouping nodes that are similar. This grouping was done based  
164 on similarities in atmospheric patterns and seasonal frequency from the 9-node case.

165

### 166 **3.2 Large-scale WAM patterns on southern West Africa MCS days**

167 Based on the 6 different large-scale node patterns, we explore within-node large-scale conditions that  
168 characterize MCS days in SWA. For examination of environmental conditions suitable for SWA MCS activity,  
169 large-scale conditions were taken from hourly ERA5 reanalysis data sampled at 1200 UTC when the daily  
170 convective activity is more representative of pre-convective atmospheric conditions (Klein et al. 2021). Pre-  
171 convective conditions are considered in the study to reduce the effects of feedback from the MCSs on environmental  
172 conditions (Song et al. 2019). Composites of ERA5 large-scale environmental variables (temperature, wind, specific  
173 humidity, and CAPE) are created for all node days, and for MCS days within each SOM node. Finally, the anomaly  
174 in large-scale patterns between MCS days and node mean conditions are computed to determine MCS-favourable  
175 adjustments in large-scale patterns within each node. A two-sided Student's t-test is used to determine significant  
176 differences between node climatologies and MCS-day sub-samples.

177 In addition to large-scale condition composites, we also sample pre-convective (1200 UTC) local  
178 atmospheric conditions (ERA5), for each 1800 UTC MCS at the location of minimum cloud top temperature. We  
179 only consider 1800 UTC MCSs for local condition sampling to avoid oversampling similar atmospheric states from  
180 several MCS time steps. These conditions are compared to the node climatology conditions at the same locations,  
181 allowing us to explore the difference in node climatology versus MCS day conditions at the specific locations where  
182 MCSs occurred on respective days.

183

184

185

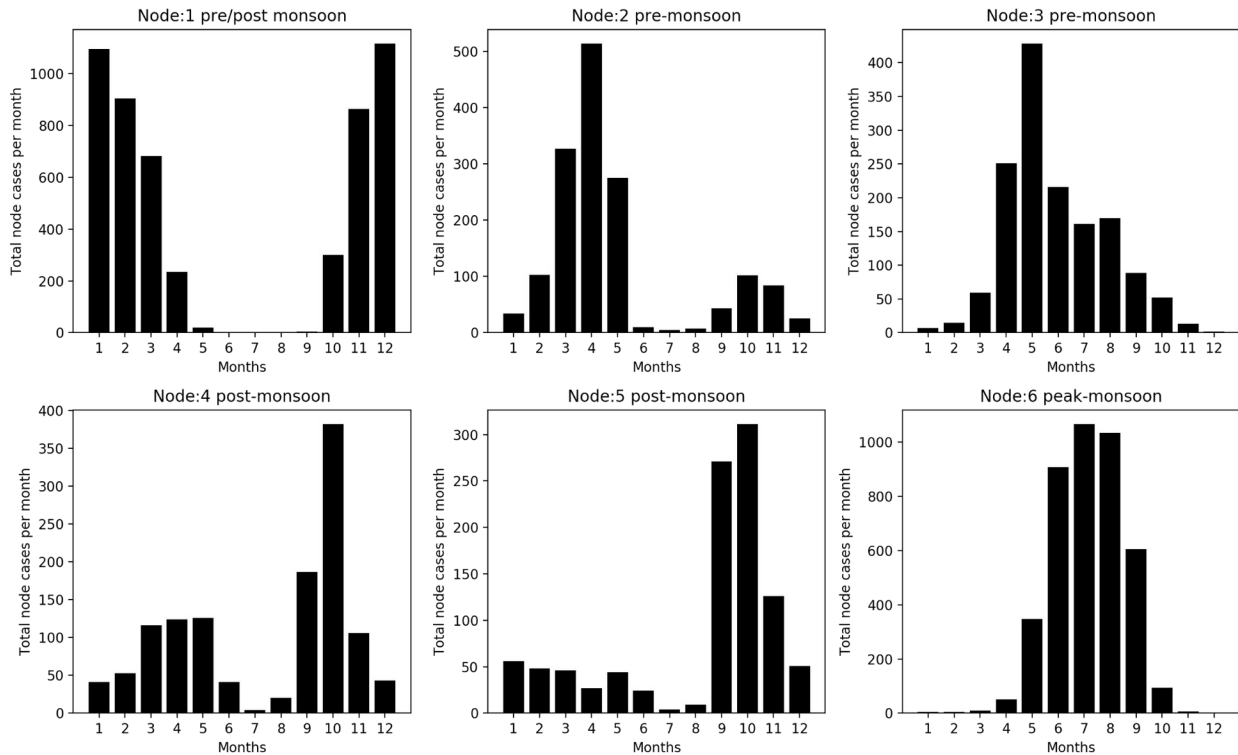
186

187 **4 Results**

188 **4.1 Node seasonality and mean conditions**

189 In analyzing the 9-node SOM (Fig. S1), six SOM nodes (Fig. 1) with distinct synoptic states were  
190 identified and were further associated with being either a pre-, post-, or peak-monsoon synoptic circulation type as a  
191 result of which months in the year they dominantly occur. This was done based on similarities in atmospheric  
192 patterns and seasonal frequency from the 3 X 3 node SOM. These nodes are hereafter referred to as nodes one (1) to  
193 six (6). The SOM nodes are noted to generally represent patterns of the seasonal cycle of monthly rainfall amounts.  
194 Circulation patterns in node 1 can be attributed to cases primarily observed in the first three months (January,  
195 February, and March) and the last two months (November, and December), hence a pattern most representative of  
196 the dry season months. It is noted that nodes 2 and 3 depict an environment that is prominent during the pre-  
197 monsoon season, with node 2 presenting a clearer seasonal exclusivity while node 3 shows frequent occurrences  
198 throughout the monsoon season. Patterns of node cases significant in the post-monsoon season are observed in nodes  
199 4 and 5. However, node 4 evidently shows transition patterns that have frequent occurrences in both pre and post-  
200 monsoon seasons although most prominent in the post-monsoon season. Patterns in node 6 are more strongly related  
201 to peak monsoon conditions.

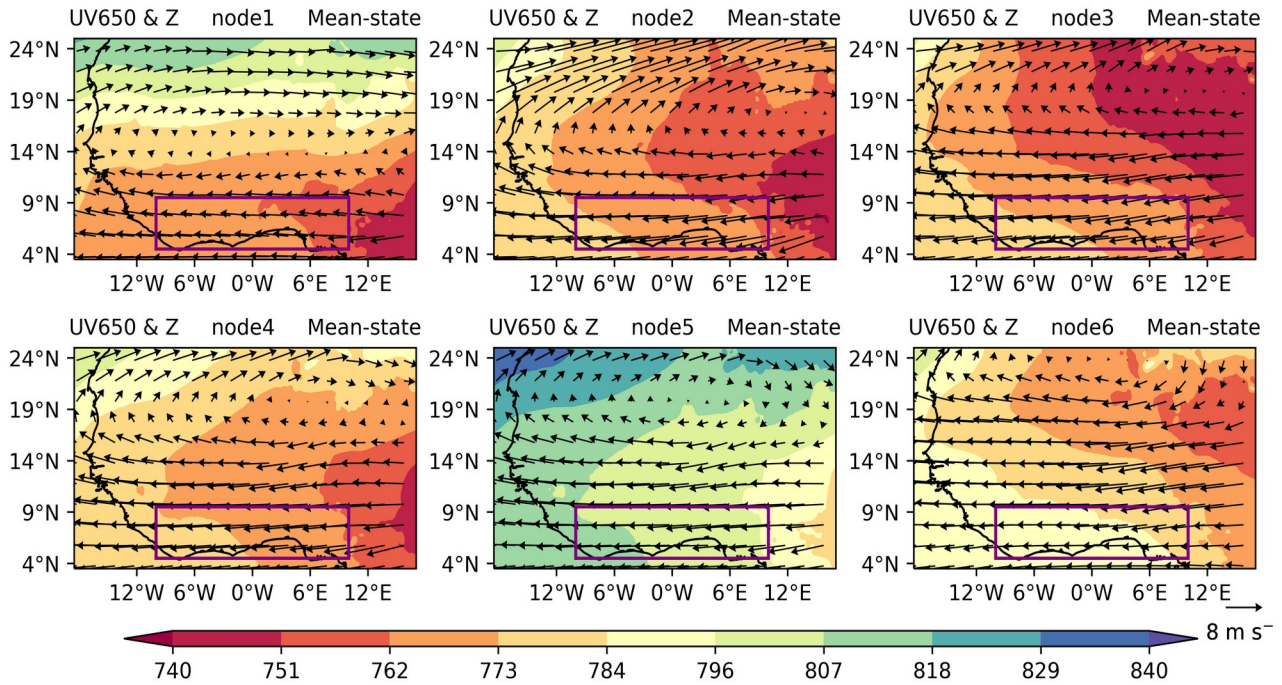
202  
203



204  
205 **Figure 1.** Monthly distribution of node cases based on SOM analysis

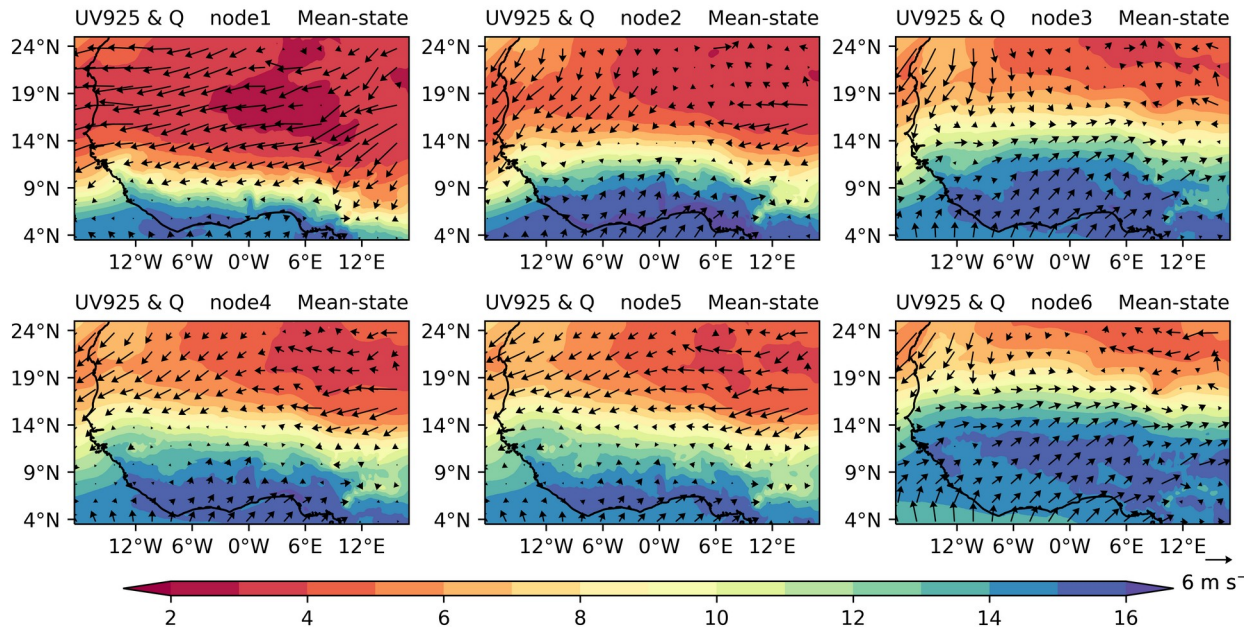
206

207 The SOM classification of different synoptic states was based on 925 hPa geopotential heights, with  
 208 resulting patterns shown in Fig. 2. The patterns clearly show the signature of the well-known West African Heat  
 209 Low (e.g. Lavaysse et al. 2009) moving northwards, strengthening over the course of the annual WAM cycle (from  
 210 nodes 1, 2, and 3) and peaking in August, evident as an area of high pressure over the Sahara in node 6. Nodes 4 and  
 211 5 show stages of the weakening of the heat low post-monsoon, coinciding with a southward movement of the 925  
 212 hPa high pressure area and linked southward retreat of mid-level easterly winds compared to node 6.  
 213  
 214



215  
 216 **Figure 2.** 12 UTC composites of 925-hPa geopotential height (shading; gpm) and 650-hPa winds (vectors;  $\text{m s}^{-1}$ ) in  
 217 six nodes based on SOM analysis. The purple box depicts the SWA region ( $5^{\circ}\text{--}9^{\circ}\text{N}$ ,  $10^{\circ}\text{W--}10^{\circ}\text{E}$ )  
 218

219 We now examine surface winds and moisture flows to explore their behaviour under the six distinct  
 220 circulation types identified (Fig. 3). In the first node, the north-easterly winds dominate most of West Africa, with  
 221 weak southerlies over SWA. This pattern in moisture distribution is evident in the dry season over West Africa,  
 222 signaling a low moisture presence. The enhanced moisture observed in coastal areas of SWA can be attributed to the  
 223 penetration of southerly winds. In pre-monsoon node 2, the southerly winds strengthen and move inland, causing the  
 224 north-easterly winds to retreat. A similar effect is observed in nodes 3, 4, and 5 where the north-easterlies become  
 225 weaker. In node 6, the south-westerlies are intensified and move inland, further enhancing moisture flow from the  
 226 South Atlantic towards the land, representative of peak monsoon flow. Wind patterns for low- and mid-levels (Figs.  
 227 2 and 3) illustrate vertically-sheared conditions coinciding with regions of high low-level specific humidity in all  
 228 nodes (purple in Fig. 3), thus marking regions where atmospheric conditions may allow MCS development.  
 229



231

232 **Figure 3.** 12 UTC composites of specific humidity (shading;  $\text{g kg}^{-1}$ ) and 925-hPa winds (vectors;  $\text{m s}^{-1}$ ) in six nodes  
 233 based on SOM analysis.

234

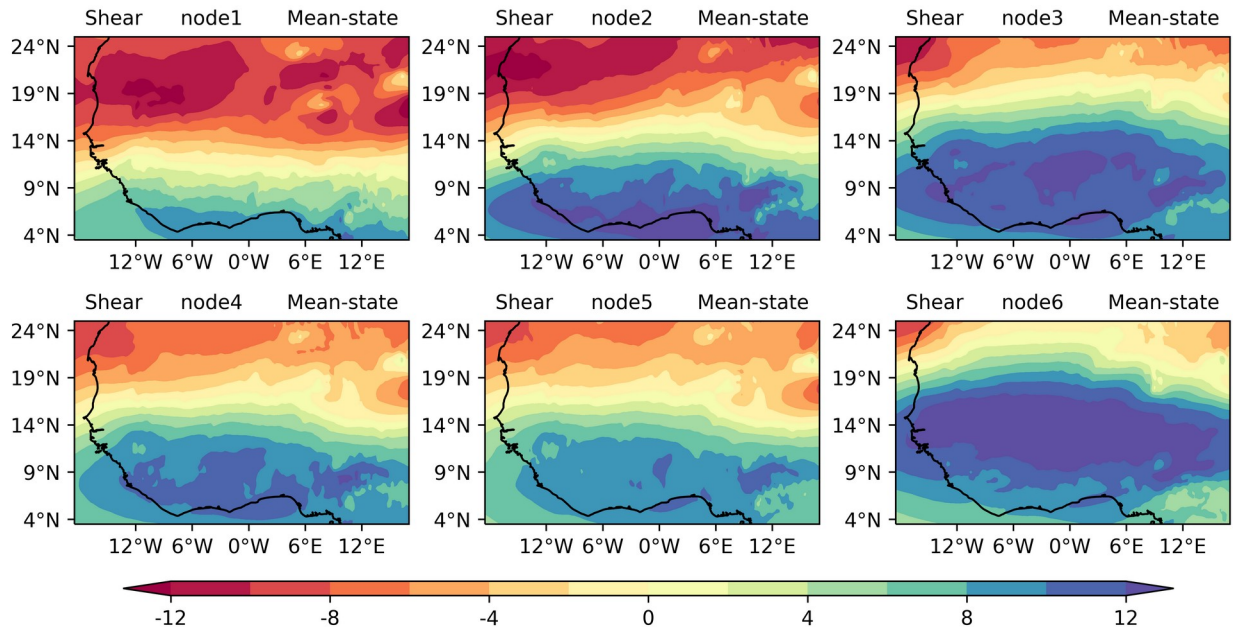
235 A further investigation was conducted to ascertain the spatial distribution of mean zonal wind shear over SWA (Fig.  
 236 4). The patterns demonstrate northward transport during the propagation of the WAM cycle and a wider spread of  
 237 zonal wind shear as it moves further inland (nodes 1, 2, and 3). These patterns closely follow the southern boundary  
 238 of weaker geopotential heights representative of high-pressure areas (Fig. 2). During the monsoon season (node 6),  
 239 zonal wind shear lies clearly to the north of the SWA domain. A southward retreat of zonal wind shear is observed  
 240 during the post-monsoon season (nodes 4 and 5). Generally, the presence of zonal wind shear can be seen as a  
 241 necessary condition in the WAM system.

242

243

244



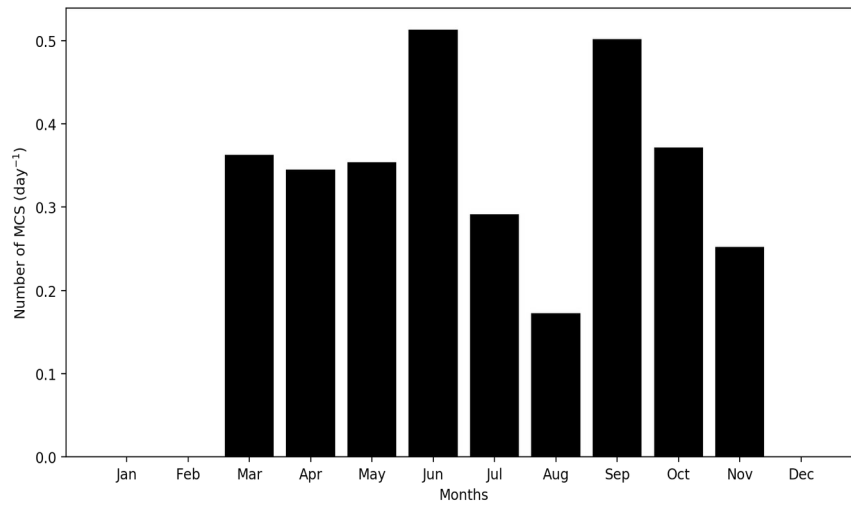


245  
 246 **Figure 4.** 12 UTC composites of zonal wind shear in six nodes based on SOM analysis.

247

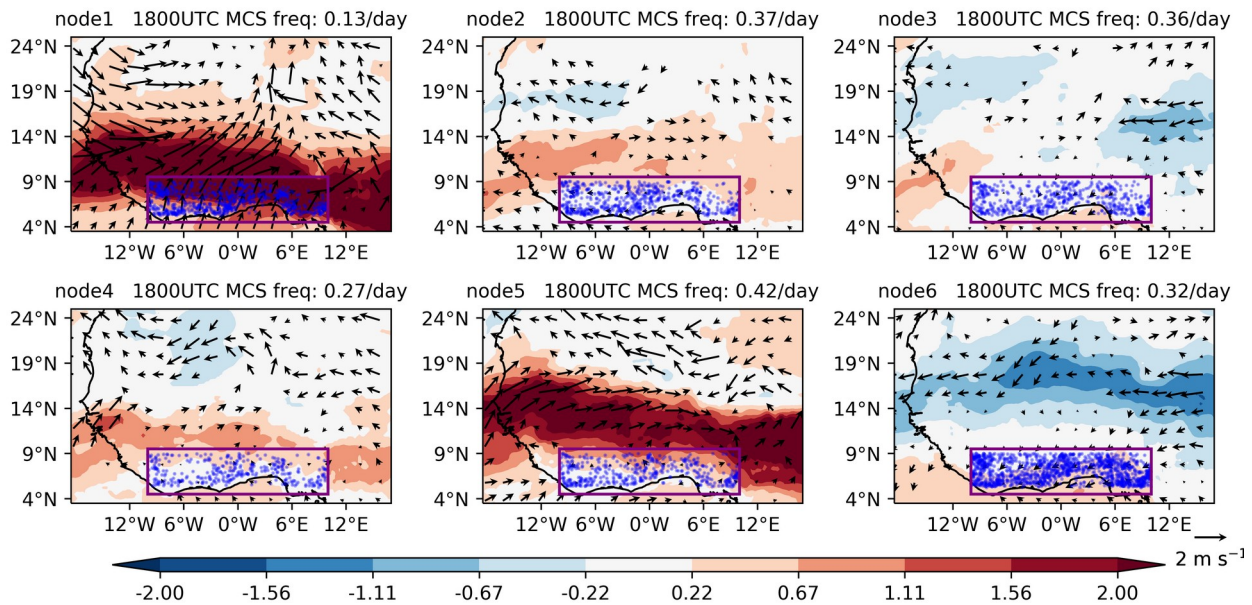
248 **4.2 Large-scale conditions favouring MCS days**

249 The environmental conditions favouring MCS occurrence are described in this section. Firstly, the monthly  
 250 climatology of MCS frequency as captured by our MCS snapshots (average number of MCSs at 1800 UTC across  
 251 SWA domain) is considered with a focus on rainfall months. A pronounced annual cycle of MCS numbers with  
 252 frequency peaks in June and September is observed (Fig. 5). These peak months are associated with maximum  
 253 rainfall during the major and minor rainy seasons across SWA respectively. The monthly climatology of MCS  
 254 frequency decreases from June to August, with August being the local minimum. This local minimum corresponds  
 255 to the so-called “little dry season” (Le Barbé et al., 2002; Vollmert et al., 2003) that exists before the southward  
 256 retreat of the rainbelt.



257 **Figure 5.** Average annual cycle of MCSs at 1800 UTC within the SWA box showing the monthly average of MCS  
 258 number per day.

259  
 260



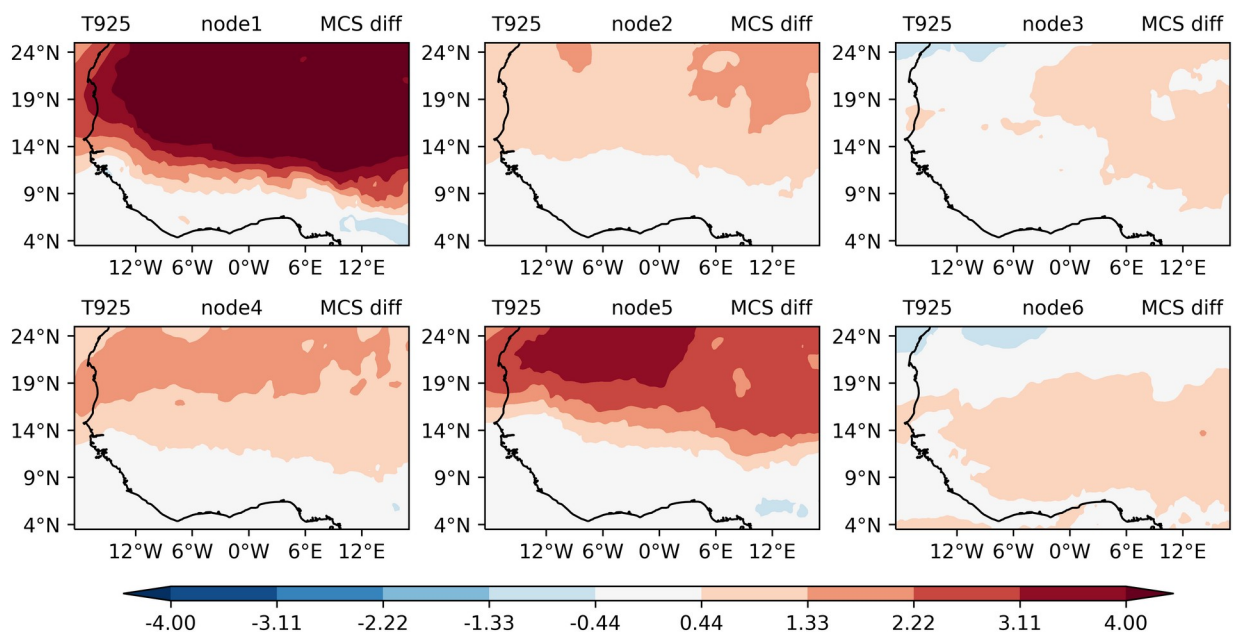
261  
 262 **Figure 6.** 12 UTC MCS-day composite anomalies of specific humidity (shading;  $\text{g kg}^{-1}$ ) and 925-hPa winds  
 263 (vectors;  $\text{m s}^{-1}$ ) in six nodes based on SOM analysis. The purple box depicts the SWA region ( $5^{\circ}$ – $9^{\circ}\text{N}$ ,  $10^{\circ}\text{W}$ – $10^{\circ}\text{E}$ )  
 264 and the blue dots indicate the location of MCSs during node days. Specific humidity anomalies are shown when they  
 265 are significant at the 5% level; wind vectors are shown when either the zonal or meridional wind anomalies are  
 266 significant at the 5% level.

267

268 In node 1, a positive widespread moisture anomaly maximum is observed with anomalous south-westerly  
 269 winds over SWA (Fig. 6). This depicts a substantial enhancement in the low-level moisture transport during days of  
 270 convective activities. In nodes 2, 3, 4, and 5, low-level moisture anomalies during convective activity days show  
 271 insignificant behaviour along the SWA coast based on the two-sided Student's t-test. In node 5, a positive moisture  
 272 anomaly is located over the northern part of SWA. In node 6, a notable region of anomalous easterly winds and also  
 273 the seemingly partly northerlies from the Mediterranean region coincides with negative moisture anomalies over the  
 274 Sahel. Strong easterly winds during MCS days reduce the moisture over the Sahel but introduce more moisture over  
 275 the coast. Comparing daily MCS frequencies, we find that MCSs are most likely to develop under node 5 conditions  
 276 featuring a northward-displaced moisture anomaly (0.42 MCSs per day), linked to strengthened low-level westerlies.  
 277 Given this node occurs predominantly from September and into November - the minor rainy season in SWA (cf.  
 278 Fig.~1), these patterns may in some cases be representative of a delayed monsoon retreat.

279 Figure 7 shows a widespread increase in temperature north of SWA during days with active convection in  
 280 nodes 1, 2, 4, and 5. The SWA region itself reveals a negative and/or insignificant change in temperature during  
 281 MCS days when compared with the mean climatology. Indeed, for nodes 1 and 5 this coincides with low-level  
 282 westerly wind south of 15N (cf. Fig. 6). In node 6, temperatures are enhanced in most parts of West Africa including  
 283 SWA.

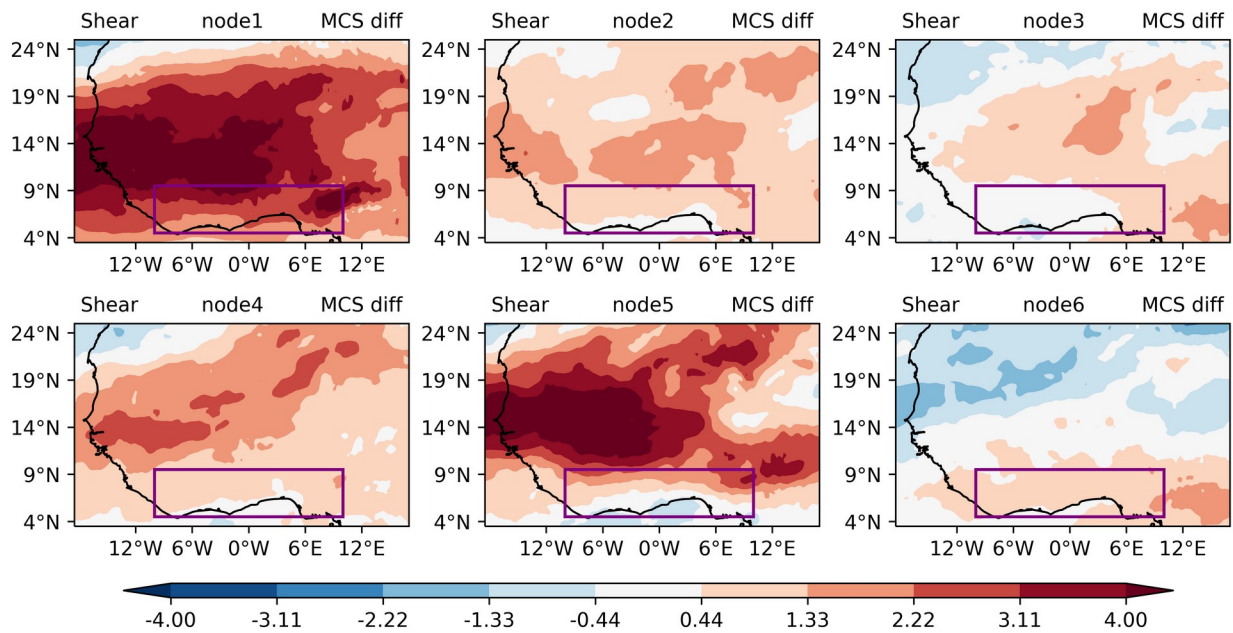
284  
 285



286  
 287 **Figure 7.** 12 UTC composite anomalies of 925hPa temperatures (°C) in six nodes based on SOM analysis.  
 288 Temperature anomalies are shown when they are significant at the 5% level.  
 289

290 Figure 8 shows the spatial distribution of zonal wind shear anomaly between days with convective MCSs  
 291 over SWA and the climatological zonal wind shear mean for the 6 different nodes across West Africa. Generally, all  
 292 nodes except node 6, reveal a widespread increase in zonal wind shear anomaly over West Africa with nodes 1 and 5  
 293 depicting stronger events. Zonal wind shear tends to be stronger during the dry and early part of the major rainy  
 294 season (node 1) with its peak partly over SWA, but resides to the north of SWA during the minor rainy season  
 295 (nodes 4 and 5), in line with previously identified zonal wind shear seasonality for the region (Klein et al. 2021).  
 296 Nodes 4 and 5 (post-monsoon) however still experience an appreciably significant increase in zonal wind shear over  
 297 SWA for MCS days during the minor rainy season. Node 6 on the other hand, exhibits a significant increase in zonal  
 298 wind shear mainly confined to SWA. In line with the expected zonal wind shear response to an increased large-scale  
 299 meridional temperature gradient, we find strongest zonal wind shear anomalies for nodes with strongest low-level  
 300 temperature anomalies to the north of SWA (nodes 1,5; followed by nodes 2,4), highlighting that a warmer Sahel  
 301 can promote MCS-favourable conditions in SWA, particularly in the pre- and post-monsoon seasons.

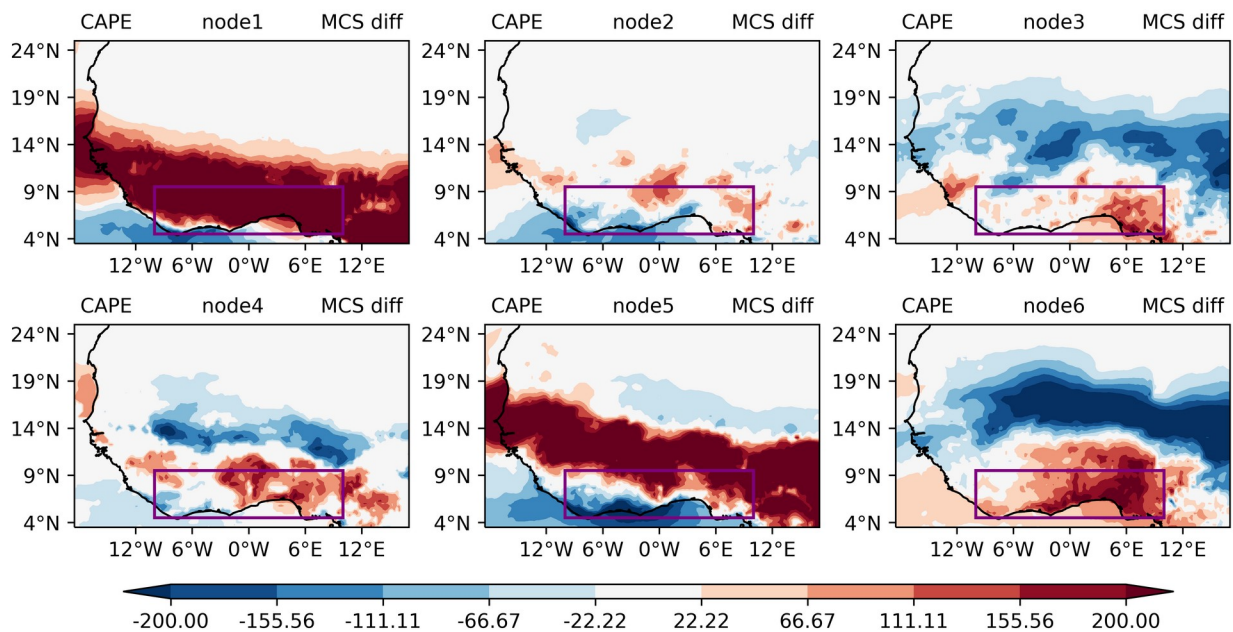
302  
 303



304  
 305 **Figure 8.** 12 UTC composite anomalies of zonal wind shear ( $\text{m s}^{-1}$ ) in six nodes based on SOM analysis. zonal wind  
 306 shear anomalies are shown when they are significant at the 5% level.

307  
 308 Investigating the first order condition for convection development, we also evaluate CAPE for a parcel at  
 309 925 hPa to ascertain the level of increased MCS-day instability in various nodes over SWA (Fig. 9). A large strip of  
 310 higher CAPE values extending over the entire region of SWA and the southern Sahel from 5°N–15°N is observed  
 311 (node 1). This large strip of higher CAPE is situated further north of SWA for node 5, while part of the western  
 312 coast tends to depict patterns of lower CAPE values, suggesting increased MCS likelihood only for eastern parts of  
 313 the domain. Node 3 shows a swath of high CAPE values in particular to the east and in some instances extends to

316 the central (node 4) and south-western parts of SWA (node 6). For nodes 3-6, higher CAPE conditions over SWA  
 317 are to differing degrees significantly associated with decreased CAPE in the Sahelian region, creating a dipole  
 318 pattern that can occur during pre-, peak- and post-monsoon periods according to node frequencies (cf. Fig 1).  
 319 Overall, all nodes show positive CAPE anomalies for MCS-days in parts of SWA, creating an environment  
 320 sufficiently unstable to support the development of convection. It can be said that regions over SWA that exhibit a  
 321 higher CAPE on MCS days also depict stronger zonal wind shear (Fig. 8). Indeed, it has previously been shown that  
 322 colder, more intense MCSs predominantly occur under conditions with high CAPE and high zonal wind shear  
 323 anomalies (Klein et al, 2021), which we show is consistent across all classified large scale patterns.  
 324  
 325

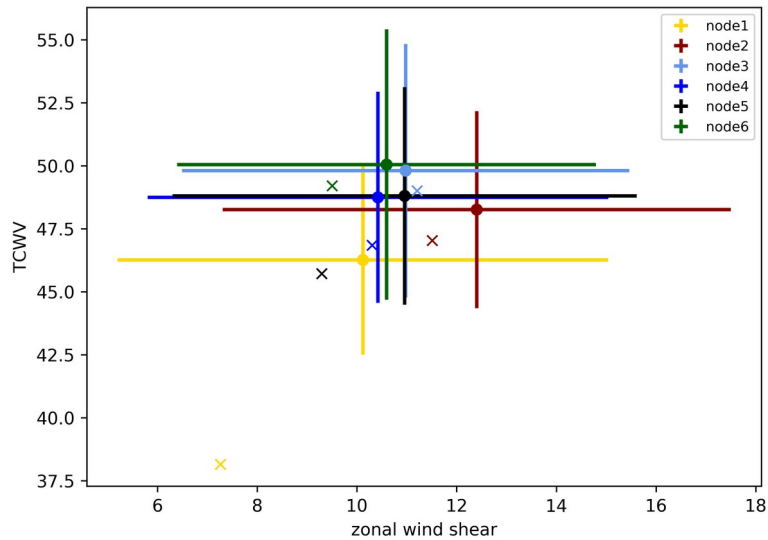


326  
 327 **Figure 9.** 12 UTC composite anomalies of CAPE ( $J\ kg^{-1}$ ) for MCSs occurring in each type of large-scale  
 328 environment determined by the SOM analysis over SWA. CAPE anomalies are shown when they are significant at  
 329 the 5% level.

330  
 331 **4.3 MCS driver variability within nodes**

332 The drivers of MCSs within different nodes are considered to examine their relative importance within the different  
 333 large-scale states (Fig. 10), concentrating on total column water vapor (TCWV) and zonal wind shear. Node 1  
 334 climatological conditions depict both, very low initial zonal wind shear and TCWV. This illustrates the relatively  
 335 low storm conditions during mean conditions for this node, predominantly representing dry season conditions and  
 336 explaining the low storm frequency of only 0.13 per day (cf. Fig. 6). Interestingly, on storm days, conditions for this  
 337 node shift to within the range of environmental conditions identified for other nodes with higher storm frequencies,  
 338 albeit node 6 MCS-day conditions still represent the lowest values in TCWV and zonal wind shear.

339  
340  
341  
342  
343  
344  
345  
346  
347  
348  
349  
350  
351



352 **Figure 10.** Mean MCS conditions over SWA for the different nodes. Dots show the mean within 1 standard  
353 deviation (whiskers) across each node. The symbol (x) denotes the mean environmental condition for all node days  
354 (MCS and non-MCS).

355

356 Pre-monsoon nodes (nodes 2 and 3) observe initial higher zonal wind shear conditions than all other nodes  
357 with appreciably higher TCWV. Node 2 observes an increase in zonal wind shear (about 1 m/s) and also a bit more  
358 TCWV. Not much change is observed in the zonal wind shear and TCWV value for node 3, making node 2 the  
359 season with relatively strong instability.. Comparing nodes 4 and 5 (both post-monsoon nodes), it can be observed  
360 that node 5 has lower zonal wind shear to start with and thus needs higher zonal wind shear change to produce MCS  
361 conditions very similar to node 4. Node 4 on the other hand shows mostly TCWV change but has a bit more zonal  
362 wind shear so, in spite of the smaller zonal wind shear anomaly (Fig. 7), the resulting MCS conditions are rather  
363 similar. Node 6 depicts an initial environmental condition of high TCWV over SWA, which is typical of periods  
364 with frequent convective activities during peak monsoon. During MCS events, there is a slight increase in zonal  
365 wind shear (about 1 m/s) and TCWV (about 0.8 kg/m<sup>2</sup>), depicting more convective activities during the monsoon  
366 season.

367

368 Generally, it can be noted that all nodes show increased TCWV on MCS days compared to their  
369 climatology. The smallest changes for both TCWV and zonal wind shear between climatology and MCS day occur  
370 for node 3, which shows the highest frequency for pre-monsoon transition month May but is still common  
371 throughout the monsoon season (c.f. Fig. 1). Together with node 4, it is also the only node for which zonal wind  
372 shear conditions remain approximately similar, but with climatological zonal wind shear strengths already reaching  
373 > 10 m/s at MCS location. Overall, node environmental conditions become more similar for MCS-days relative to  
374 the climatologies, illustrating that favourable MCS conditions converge towards high TCWV (affecting CAPE), and  
high zonal wind shear environments irrespective of the large-scale situation.

## 375 5 Conclusion

376 The study identified six synoptic states and then examined what changes are associated with favourable  
377 MCS environments in Southern West Africa under these states. For the definition of synoptic states and MCS days,  
378 we used self-organizing maps (SOM) based on ERA5 geopotential height data and 12 years of tracked MCSs using  
379 Meteosat Second Generation (MSG) 10.8  $\mu\text{m}$ -band brightness temperature data (2004-15), respectively. The  
380 identified synoptic states based on the SOM nodes are noted to generally represent patterns of the seasonal rainfall  
381 cycle. Circulation patterns in node 1 can be attributed to cases primarily observed in the dry season months (January,  
382 February, November, and December). An environment representative of the pre-monsoon season is depicted by  
383 nodes 2 and 3, with node 2 presenting a clearer seasonal exclusivity. Patterns of the post-monsoon season are  
384 observed in nodes 4 and 5 with node 4 evidently depicting transition patterns that have frequent occurrences in both  
385 pre and post-monsoon seasons although prominent in the post-monsoon season. Peak monsoon conditions are  
386 clearly represented in node 6 with large-scale conditions occurring mainly in June, July, and August. The south-  
387 westerly winds observed over SWA are strengthened and move inland, enhancing moisture flow from the South  
388 Atlantic towards the land during the peak monsoon. In the pre-monsoon and post-monsoon seasons, similar but  
389 weakened south-westerly circulation patterns are observed. The synoptic-state-related MCSs realize a pronounced  
390 annual cycle of MCS numbers with frequency peaks in June and September. These peak months are well associated  
391 with maximum rainfall during the major and minor rainy seasons across SWA respectively. During the course of the  
392 year, MCSs are most likely to develop under post-monsoon conditions featuring a northward-displaced moisture  
393 anomaly (0.42 MCSs per day) which is associated with strengthened low-level westerlies, and in some cases may be  
394 representative of a delayed monsoon retreat. Furthermore, the strongest zonal wind shear anomalies over SWA are  
395 realized in seasons with the strongest low-level temperature anomalies to the north of SWA, representative of  
396 favourable MCS conditions in SWA during periods of a warmer Sahel. Regions over SWA that show stronger zonal  
397 wind shear on MCS days also depict higher CAPE. We found node environmental conditions to become more  
398 similar for MCS-days relative to the node climatologies, illustrating that favourable MCS conditions converge  
399 towards high TCWV/high zonal wind shear states. Overall, our results show that MCSs develop on average in  
400 similar high moisture, high zonal wind shear local environments under all large-scale situations throughout the year.  
401 The latter however defines the frequency at which favourable MCS environments can occur.

402

403 *Code and data availability.* Codes for the findings of this study are available upon reasonable request from the  
404 authors. The processing of ERA5 data made direct access to the primary data archive held at ECMWF, and is  
405 available from the Copernicus Data Store (<https://cds.climate.copernicus.eu/>) and the MSG data are available from  
406 <http://www.eumetsat.int>.

407

408 *Author contributions.* FN, NABK and CK conceptualized the study, with input from KAQ; All authors contributed  
409 to and discussed the methodological design, and analyses were conducted by FN and CK; FN, ROB and KAQ wrote  
410 the manuscript draft; CK, NABK, PE, GMLDQ and HAK reviewed and edited the manuscript.

411

412 *Competing interests.* The contact author has declared that none of the authors has any competing interests.

413 *Acknowledgments.* This work is supported by a grant from the Government of Canada, provided through Global  
414 Affairs Canada, [www.international.gc.ca](http://www.international.gc.ca) (accessed on 1 January 2021), and the International Development Research  
415 Centre, [www.idrc.ca](http://www.idrc.ca), (accessed on 1 June 2022) to the African Institute for Mathematical Sciences—Next Einstein  
416 Initiative (AIMS-NEI) [Number: 108246-001]. CK acknowledges funding from the NERC-funded LMCS project  
417 (NE/W001888/1). KQ also acknowledges funding from the National Research Foundation (NRF), South Africa.

## 418 **References**

- 419 Alfaro, D. A.: Low-Tropospheric Shear in the Structure of Squall Lines: Impacts on Latent Heating under Layer-  
420 Lifting Ascent, *J Atmos Sci.*, 74, 229–48, <https://doi.org/10.1175/JAS-D-16-0168.1>, 2017.
- 421 Augustin, D., Pascal, I.M., Jores, T.K., Elisabeth, F.D., Cesar, M.B., Michael, T.F., Roméo-Ledoux, D.T.,  
422 Marceline, M., Gladys, K.N.F. and Firmin, B.A.: Impact Assessment of the West African Monsoon on  
423 Convective Precipitations over the Far North Region of Cameroon, *Adv. Space Res.*,  
424 <https://doi.org/10.1016/j.asr.2022.04.044>, 2022.
- 425 Baidu, M., Schwendike, J., Marsham, J.H. and Bain, C.: Effects of Vertical Wind Shear on Intensities of Mesoscale  
426 Convective Systems over West and Central Africa, *Atmos. Sci. Lett.*, e1094, <https://doi.org/10.1002/asl.1094>,  
427 2022.
- 428 Biasutti, M., Sobel, A. H., & Camargo, S. J.: The role of the Sahara low in summertime Sahel rainfall variability and  
429 change in the CMIP3 models. *Journal of Climate*, 22(21), 5755-5771,  
430 <https://doi.org/10.1175/2009JCLI2969.1>, 2009.
- 431 Cassano, E.N., Glisan, J.M., Cassano, J.J., Gutowski Jr, W.J. and Seefeldt, M.W.: Self-Organizing Map Analysis of  
432 Widespread Temperature Extremes in Alaska and Canada, *Clim. Res.* 62, 199-218,  
433 <https://doi.org/10.3354/cr01274>, 2015.
- 434 Chen, Y., Luo, Y. and Liu, B.: General Features and Synoptic-Scale Environments of Mesoscale Convective  
435 Systems over South China during the 2013-2017 Pre-Summer Rainy Seasons, *Atmos. Res.*, 266,  
436 <https://doi.org/10.1016/j.atmosres.2021.105954>, 2022.
- 437 Feng, Z., Leung, L.R., Liu, N., Wang, J., Houze Jr, R.A., Li, J., Hardin, J.C., Chen, D. and Guo, J. A.: Global High-  
438 Resolution Mesoscale Convective System Database Using Satellite-Derived Cloud Tops, Surface  
439 Precipitation, and Tracking, *J. Geophys. Res. Atmos.* 126, e2020JD034202,  
440 <https://doi.org/10.1029/2020JD034202>, 2021.
- 441 Guo, Y., Du, Y., Lu, R., Feng, X., Li, J., Zhang, Y. and Mai, Z.: The Characteristics of Mesoscale Convective  
442 Systems Generated over the Yunnan-Guizhou Plateau during the Warm Seasons, *Int. J. Climatol.*,  
443 <http://doi.org/10.1002/joc.7647>, 2022.
- 444 Guy, N., Rutledge, S.A. and Cifelli, R.: “Radar Characteristics of Continental, Coastal, and Maritime Convection  
445 Observed during AMMA/NAMMA”, *Q. J. R. Meteorol. Soc.* 137, 1241-56, <http://doi.org/10.1002/qj.839>,  
446 2011.
- 447 Hewitson, B. C., & Crane, R. G.: *Climate Downscaling: Techniques and Application.* *Clim. Res.* 7, 85-95,  
448 <https://doi.org/10.3354/cr007085>, 1996.



- 449 Hewitson, B. C., & Crane, R. G. “Self-Organizing Maps: Applications to Synoptic Climatology.” *Clim. Res.* 22, 13-  
450 26, <https://doi.org/10.3354/cr022013>, 2002.
- 451 Hodges, K.I. and Thorncroft, C.D.: Distribution and Statistics of African Mesoscale Convective Weather Systems  
452 Based on the ISCCP Meteosat Imagery, *Mon Weather Rev* 125, 2821-37, [https://doi.org/10.1175/1520-  
453 0493\(1997\)125<2821:DASOAM>2.0.CO;2](https://doi.org/10.1175/1520-0493(1997)125<2821:DASOAM>2.0.CO;2), 1997.
- 454 Houze Jr, Robert A.: Mesoscale Convective Systems”, *Rev. Geophys.*, 42, <http://doi.org/10.1029/2004RG000150>,  
455 2004.
- 456 Hussain, M.S., Kim, S. and Lee, S.: On the Relationship between Indian Ocean Dipole Events and the Precipitation  
457 of Pakistan, *Theor. Appl. Climatol.* 130, 673-85, <http://doi.org/10.1007/s00704-016-1902-y>, 2017.
- 458 IPCC: Climate Change, 2014: Synthesis Report. Contribution of Working groups I, II, and III to the Fifth  
459 Assessment Report of the Intergovernmental Panel on Climate Change [Core Working Team, R.K. Pachauri  
460 and L.A. Meyer (eds)]. IPCC, Geneva, Switzerland, 151, 2014
- 461 Janiga, M.A. and Thorncroft, C.D.: The Influence of African Easterly Waves on Convection over Tropical Africa  
462 and the East Atlantic, *Mon Weather Rev* 144, 171-92, <https://doi.org/10.1175/MWR-D-14-00419.1>, 2016.
- 463 Kamara, S. I.: The Origins and Types of Rainfall in West Africa, *Weather* 41, 48-56, [https://doi.org/10.1002/j.1477-  
464 8696.1986.tb03787.x](https://doi.org/10.1002/j.1477-8696.1986.tb03787.x), 1986.
- 465 Kim, H.K. and Seo, K.H.: Cluster Analysis of Tropical Cyclone Tracks over the Western North Pacific Using a Self-  
466 Organizing Map, *JCLI* 29, 3731-51, <https://doi.org/10.1175/JCLI-D-15-0380.1>, 2016.
- 467 Klein, C., Belušić, D., & Taylor, C. M.: Wavelet scale analysis of mesoscale convective systems for detecting deep  
468 convection from infrared imagery. *Journal of Geophysical Research: Atmospheres*, 123, 3035 - 3050.  
469 <https://doi.org/10.1002/2017JD027432>, 2018.
- 470 Klein, C., Nkrumah, F., Taylor, C.M. and Adefisan, E.A.: Seasonality and Trends of Drivers of Mesoscale  
471 Convective Systems in Southern West Africa, *JCLI* 34, 71-87, <https://doi.org/10.1175/JCLI-D-20-0194.1>,  
472 2021.
- 473 Kohonen, T. “Self-Organizing Maps.-Springer Series in Information Sciences, V. 30, Springer Sci. Rev.,  
474 <https://doi.org/10.1007/978-3-642-56927-2>, 2001.
- 475 Kusangaya, S., Warburton, M.L., Van Garderen, E.A. and Jewitt, G.P.: Impacts of Climate Change on Water  
476 Resources in Southern Africa: A Review, *Phys. Chem. Earth.*, 47-54,  
477 <https://doi.org/10.1016/j.pce.2013.09.014>, 2014.
- 478 Laing, A.G., Carbone, R., Levizzani, V. and Tuttle, J.: The Propagation and Diurnal Cycles of Deep Convection in  
479 Northern Tropical Africa, *Q J R Meteorol Soc.* 134, 93-109, <http://doi.org/10.1002/qj.194>, 2008.
- 480 Lavaysse, C., Flamant, C., Janicot, S., Parker, D.J., Lafore, J.P., Sultan, B. and Pelon, J.: Seasonal Evolution of the  
481 West African Heat Low: A Climatological Perspective, *Clim. Dyn.* 33, 313-30,  
482 <https://doi.org/10.1007/s00382-009-0553-4>, 2009.
- 483 Le Barbé, L., Lebel, T., & Tapsoba, D.: Rainfall variability in West Africa during the years 1950 - 90. *J. Clim.*  
484 15(2), 187-202, [https://doi.org/10.1175/1520-0442\(2002\)015<0187:RVIWAD>2.0.CO;2](https://doi.org/10.1175/1520-0442(2002)015<0187:RVIWAD>2.0.CO;2), 2002.
- 485 Li, P., Moseley, C., Prein, A.F., Chen, H., Li, J., Furtado, K. and Zhou, T.: Mesoscale Convective System  
486 Precipitation Characteristics over East Asia. Part I: Regional Differences and Seasonal Variations, *J. Clim.*  
487 33, 9271-86, <https://doi.org/10.1175/JCLI-D-20-0072.1>, 2020.

488 Maranan, M., Fink, A.H. and Knippertz, P.: Rainfall Types over Southern West Africa: Objective Identification,  
489 Climatology and Synoptic Environment, Q J R Meteorol Soc. 144, 1628-48, <https://doi.org/10.1002/qj.3345>,  
490 2018.

491 Mohr, K. I., and Zipser, E. J.: Mesoscale convective systems defined by their 85-GHz ice scattering signature: Size  
492 and intensity comparison over tropical oceans and continents. *Mon. Wea. Rev.*, 124, 2417-2437,  
493 [https://doi.org/10.1175/1520-0493\(1996\)124<2417:MCSDBT>2.0.CO;2](https://doi.org/10.1175/1520-0493(1996)124<2417:MCSDBT>2.0.CO;2), 1996

494 Mohr, K.I. and Thorncroft, C.D.: Intense Convective Systems in West Africa and Their Relationship to the African  
495 Easterly Jet, Q J R Meteorol Soc. 132, 163-76, <https://doi.org/10.1256/qj.05.55>, 2006.

496 Nesbitt, S.W., Cifelli, R. and Rutledge, S.A.: Storm Morphology and Rainfall Characteristics of TRMM  
497 Precipitation Features, *Mon Weather Rev* 134, 2702-21, <https://doi.org/10.1175/MWR3200.1>, 2006.

498 Queralt, S., Hernández, E., Barriopedro, D., Gallego, D., Ribera, P. and Casanova, C.: North Atlantic Oscillation  
499 Influence and Weather Types Associated with Winter Total and Extreme Precipitation Events in Spain,  
500 *Atmos. Res.* 94, 675-83, <https://doi.org/10.1016/j.atmosres.2009.09.005>, 2009.

501 Schmetz, J., Pili, P., Tjemkes, S., Just, D., Kerkmann, J., Rota, S. and Ratier, A.: An Introduction to Meteosat  
502 Second Generation (MSG)", *Bull Am Meteorol Soc* 83, 977-92, [https://doi.org/10.1175/1520-0477\(2002\)083<0977:AITMSG>2.3.CO;2](https://doi.org/10.1175/1520-0477(2002)083<0977:AITMSG>2.3.CO;2), 2002.

504 Schrage, J.M., Fink, A.H., Ermert, V. and Ahlonsou, E.D.: Three MCS Cases Occurring in Different Synoptic  
505 Environments in the Sub-Sahelian Wet Zone during the 2002 West African Monsoon, *J Atmos Sci* 63, 2369-  
506 82, <https://doi.org/10.1175/JAS3757.1>, 2006.

507 Sheridan, S. and Lee, C.C.: Synoptic Climatology and the Analysis of Atmospheric Teleconnections, *Prog Phys*  
508 *Geogr.* 36, 548-57, <https://doi.org/10.1177/0309133312447935>, 2012.

509 Sultan, B., & Janicot, S.: The West African monsoon dynamics. Part II: The "preonset" and "onset" of the summer  
510 monsoon. *Journal of climate*, 16(21), 3407-3427, [https://doi.org/10.1175/1520-0442\(2003\)016<3407:TWAMDP>2.0.CO;2](https://doi.org/10.1175/1520-0442(2003)016<3407:TWAMDP>2.0.CO;2), 2003.

512 Taylor, C.M., Belušić, D., Guichard, F., Parker, D.J., Vischel, T., Bock, O., Harris, P.P., Janicot, S., Klein, C. and  
513 Panthou, G.: Frequency of Extreme Sahelian Storms Tripled since 1982 in Satellite Observations, *Nature* 544,  
514 475-78, <https://doi.org/10.1038/nature22069>, 2017.

515 Thorncroft, Chris D, Hanh Nguyen, Chidong Zhang, and Philippe Peyrillé.: Annual Cycle of the West African  
516 Monsoon: Regional Circulations and Associated Water Vapour Transport, *Q. J. R. Meteorol. Soc.* 137, 129-  
517 47, <https://doi.org/10.1002/qj.728>, 2011.

518 Vizy, E.K. and Cook, K.H.: Mesoscale Convective Systems and Nocturnal Rainfall over the West African Sahel:  
519 Role of the Inter-Tropical Front, *Clim. Dyn.* 50, 587-614, <https://doi.org/10.1007/s00382-009-0553-4>, 2018.

520 Wolski, P., Jack, C., Tadross, M., van Aardenne, L. and Lennard, C.: Interannual Rainfall Variability and SOM-  
521 Based Circulation Classification", *Clim. Dyn.* 50, 479-92, <https://doi.org/10.1007/s00382-017-3621-1>, 2018.

522